Self-diffusion in a periodic porous medium with interface absorption

David J. Bergman* and Keh-Jim Dunn
Chevron Petroleum Technology Company, P.O. Box 446, La Habra, California 90633-0446
(Received 4 October 1994)

A matrix eigenvalue problem for the diffusion eigenstates of a periodic porous medium with interface absorption is set up by expanding those eigenstates in terms of the eigenstates of the zero absorption diffusion problem in the same medium. This approach enables us to obtain accurate numerical solutions for many aspects of self-diffusion. We use our approach to evaluate the time-dependent bulk effective or restricted diffusion coefficient of the fluid filled porous medium and other properties that can be measured using NMR techniques, such as the spectrum of spin relaxation times and the spin echo amplitude in the presence of a pulsed magnetic field gradient.

PACS number(s): 47.55.Mh, 05.60.+w, 07.57.Pt, 66.10.Cb

I. INTRODUCTION

In 1966, Wayne and Cotts studied particle diffusion in a restricted geometry using nuclear spin echo measurements in the presence of a fixed magnetic field gradient [1]. More recently, spin echo measurements in the presence of a pulsed field gradient have been shown to be capable of yielding even more detailed information about diffusion in such systems [2–5]. Much of the interest in these experimental techniques is due to possible applications in biology and medicine, where these methods allow *in vivo* measurements which are noninvasive as well as radiation free [5]. The ability to perform measurements without having to have a specially prepared sample inside the measurement apparatus is also attractive for geological studies and oil exploration. There, instruments are often physically restricted to lie in a long and deep borehole whereas the material under investigation (e.g., fluid filled porous rock) lies some distance away [6]. It is therefore no surprise that some effort has also been invested in theoretical studies of diffusion in a porous medium, with special emphasis on how the restricted diffusion affects quantities such as the spin echo amplitude [7–15].

A useful quantity, which contains all the information about self-diffusion in the porous medium, is the diffusion propagator $G(\mathbf{r},\mathbf{r}',t)$, which satisfies the following equations

$$\frac{\partial G}{\partial t} = D_p \nabla^2 G \quad \text{in the pore space,} \tag{1.1}$$

$$\frac{\partial G}{\partial n} + \frac{\rho}{D_p} G = 0 \quad \text{at the pore-matrix interface,} \tag{1.2}$$

$$G|_{t=0} = \delta^3(\mathbf{r}-\mathbf{r}'). \tag{1.3}$$

Here $D_p > 0$ is the diffusion coefficient in the pore space and $\rho \geq 0$ is a coefficient that characterizes the rate of absorption at the pore-matrix interface. In the case of diffusing molecules that carry an oriented or polarized nuclear magnetic moment, this absorption really represents an enhanced surface relaxation of the spin orientation. The enhanced relaxation is usually caused by nonmobile paramagnetic ions adsorbed at the interface.

In a pulsed-field-gradient–spin-echo (PFGSE) experiment, a spatially uniform gradient of the magnetic field ∇H is applied for a short duration of time δ during both the decay period of the spin precession signal and the subsequent reconstitution period, when the spin echo signal is being built up. The measured echo in such an experiment, also called the PFGSE amplitude, is given by a double spatial Fourier transform of G (see, e.g., Refs. [12,13])

$$M(\mathbf{k},t) \equiv \frac{1}{V_p}\int_{V_p} dV \int_{V_p} dV' G(\mathbf{r},\mathbf{r}',t) e^{-i\mathbf{k}\cdot(\mathbf{r}-\mathbf{r}')}, \tag{1.4}$$

where t is the time separation between the field gradient pulses, V_p is the total volume of the pore space, and the wave vector $\mathbf{k}$ is simply related to ∇H, δ, and the gyromagnetic ratio of the diffusing molecule γ

$$\mathbf{k} = \gamma \delta \nabla H. \tag{1.5}$$

In some of the recent theoretical studies, considerable effort was devoted to developing approximate methods for calculating G and M, as well as the values of the bulk effective, time-dependent, microgeometry restricted diffusion coefficient $D(t)$ [12–15], which is defined for an isotropic porous medium (also for a porous medium with cubic point symmetry) by focusing on the small $\mathbf{k}$ behavior of $M(\mathbf{k},t)$ and writing

$$M(\mathbf{k},t) \equiv M(\mathbf{0},t) e^{-\mathbf{k}^2 D(t) t}, \quad |\mathbf{k}|a \ll 1, \tag{1.6}$$

where a is a typical linear size scale of the pore structure. As $t \to \infty$ (i.e., when $t \gg a^2/D_p$), $D(t)$ tends to a limiting value denoted by D_e, which is the bulk effective or macroscopic diffusion coefficient of the fluid filled

*Permanent address: School of Physics and Astronomy, Raymond and Beverly Sackler Faculty of Exact Sciences, Tel Aviv University, Tel Aviv 69978, Israel.

porous medium. For times t such that $t \ll a^2/D_p$, explicit asymptotic expressions have been evolved for $D(t)$ that allow it to be calculated from a knowledge of D_p, ρ, and the surface-to-volume ratio S_p/V_p of the total pore space [14].

When we consider (1.4), the intrinsic relaxation rate of magnetization in the bulk pore fluid is already factored out, therefore when $\rho = 0$, we get that the total magnetization $M(\mathbf{0},t)$ has the constant value 1 for all times t. When $\rho \neq 0$, $M(\mathbf{0},t)$ acquires a nontrivial time dependence and decreases with increasing time due to the interface enhanced relaxation. This decay can be described by a linear combination of decaying exponentials. To these interface enhanced decay rates one should add the intrinsic decay rate of magnetic polarization in the bulk pore fluid. In practice, the interface enhanced relaxation rates are usually much greater than the intrinsic rate and in that case the spectrum of relaxation rates is essentially determined by the surface relaxation. That is why, by performing PFGSE experiments and using either (1.4) or (1.6), important and detailed information can be garnered regarding the process of restricted diffusion in a fluid filled porous medium.

In a recent article [16], we proposed an approach for studying restricted diffusion in a *periodic* porous medium with *zero interface absorption* (i.e., $\rho = 0$). In that approach, the diffusion eigenstates are first calculated numerically by solving a matrix eigenvalue problem for the Fourier expansion coefficients of the eigenfunctions. The eigenstates are then used to calculate other quantities, such as G, M, and $D(t)$. This is considerably less trivial than it may sound because at the outset these eigenfunctions were not defined everywhere, but only inside the pore space, and their normal derivative was required to vanish at the pore-matrix interface. This was dealt with by rewriting the diffusion equation as an equation for the *local chemical potential*, which is defined everywhere, unlike the equation for the *particle density*, which is only nonzero inside the pore space and has a jump discontinuity at the pore-matrix interface. This extension of the equation to the *entire volume* of pore space plus matrix had the effect of incorporating the above mentioned boundary condition into the revised differential equation for the diffusion.

In this article we broaden that discussion to the case of diffusion in a periodic porous medium with *nonzero interface absorption* (i.e., $\rho \neq 0$). This is achieved by expanding the eigenstates of the $\rho \neq 0$ problem in terms of those of the $\rho = 0$ problem and setting up a matrix eigenvalue problem for the expansion coefficients. The method is applied to a number of systems, with different porosities, made by embedding a periodic, simple cubic array of identical spherical obstacles inside an otherwise uniform fluid. These systems include cases where there is some overlap between neighboring obstacles as well as cases where neighboring obstacles are well separated. This calculational method, like its predecessor in Ref. [16], is applicable to any type of microstructure, with whatever value of the porosity, as long as it is composed of a unit cell which is repeated in a periodic fashion.

The remainder of this article is organized as follows. In Sec. II we describe the theory and discuss some practical aspects of its implementation. In Sec. III we present results for the eigenstates, the bulk effective time-dependent diffusion coefficient, the nuclear spin relaxation rate, and the PFGSE amplitude in a number of sample systems. In Sec. IV we present some conclusions and suggestions for further work. In Appendix A we discuss some of the more technical aspects of the Fourier expansion which affect our results. In Appendix B we present some results of a perturbation analysis applied to the restricted diffusion problem. In Appendix C we present some short time asymptotic expressions for $D(t)$.

II. THEORY

The diffusion eigenstates of a porous medium are solutions of the eigenvalue problem

$$\mu\psi_\mu + D_p\nabla^2\psi_\mu = 0 \quad \text{inside the pore space,} \tag{2.1}$$

$$\frac{\partial\psi_\mu}{\partial n} + \frac{\rho}{D_p}\psi_\mu = 0 \quad \text{at the pore-matrix interface.} \tag{2.2}$$

Here μ is the eigenvalue and $\psi_\mu(\mathbf{r})$ the eigenfunction. It is easily shown that the eigenvalues are all real and strictly positive whenever ρ is strictly positive and eigenfunctions that correspond to different eigenvalues are mutually orthogonal and can be normalized to 1, namely,

$$\int_{V_p} dV\psi_\mu^*\psi_\nu = \delta_{\mu\nu}. \tag{2.3}$$

Like any other function, the diffusion propagator $G(\mathbf{r},\mathbf{r}',t)$ can be expanded in the complete set of states $\{\psi_\mu\}$

$$G(\mathbf{r},\mathbf{r}',t) = \sum_\mu e^{-\mu t}\psi_\mu(\mathbf{r})\psi_\mu^*(\mathbf{r}'). \tag{2.4}$$

In general, for a disordered pore structure, the spectrum of eigenvalues is quasicontinuous and the sum that appears in this expression is really an integral.

We wish to expand these eigenstates in terms of the eigenstates of the same medium but *without any interface absorption*, i.e., in terms of the $\rho = 0$ eigenstates. The eigenvalues and eigenfunctions of the latter problem are denoted by $\lambda, \phi_\lambda(\mathbf{r})$ and they are solutions of

$$\lambda\phi_\lambda + D_p\nabla^2\phi_\lambda = 0 \quad \text{inside the pore space,} \tag{2.5}$$

$$\frac{\partial\phi_\lambda}{\partial n} = 0 \quad \text{at the pore-matrix interface.} \tag{2.6}$$

Using Green's theorem and the appropriate boundary conditions at the pore-matrix interface, the overlap integral between a ψ function and a ϕ function can be transformed in two different ways: by using either (2.1) and (2.2) or (2.5) and (2.6). These transformations lead, respectively, to

$$\mu\int_{V_p} dV\phi_\lambda^*\psi_\mu = D_p\int_{V_p} dV\boldsymbol{\nabla}\phi_\lambda^*\cdot\boldsymbol{\nabla}\psi_\mu + \rho\oint_{\partial V_p} dS\phi_\lambda^*\psi_\mu, \tag{2.7}$$

$$\lambda \int_{V_p} dV \phi_\lambda^* \psi_\mu = D_p \int_{V_p} dV \nabla \phi_\lambda^* \cdot \nabla \psi_\mu, \tag{2.8}$$

where ∂V_p is the pore-matrix interface, whose total area is denoted by S_p. These equations are combined to yield

$$(\mu - \lambda) \int_{V_p} dV \phi_\lambda^* \psi_\mu = \rho \oint_{\partial V_p} dS \phi_\lambda^* \psi_\mu. \tag{2.9}$$

The expansion of ψ_μ in terms of the ϕ_λ

$$\psi_\mu = \sum_\lambda A_\lambda^{(\mu)} \phi_\lambda, \tag{2.10}$$

when substituted in (2.9), leads to an equation for the expansion coefficients $A_\lambda^{(\mu)}$

$$(\mu - \lambda) A_\lambda^{(\mu)} = \rho \sum_\nu V_{\lambda\nu} A_\nu^{(\mu)}, \tag{2.11}$$

$$V_{\lambda\nu} \equiv \oint_{\partial V_p} dS \phi_\lambda^* \phi_\nu, \tag{2.12}$$

where we assumed that the ϕ_λ functions are normalized just like the ψ_μ functions [see (2.3)]. This is a matrix eigenvalue problem where the matrix elements are determined by the eigenstates of the $\rho = 0$ diffusion problem. Note that the $\lambda = 0$ eigenfunction of the $\rho = 0$ diffusion problem is a constant

$$\phi_0(\mathbf{r}) = \frac{1}{\sqrt{V_p}}, \tag{2.13}$$

therefore the matrix element V_{00} is always equal to the surface-to-volume ratio of the total pore space

$$V_{00} = \frac{S_p}{V_p}. \tag{2.14}$$

Because the spectrum of $\rho = 0$ eigenstates is in general continuous, the sum in (2.11) is usually an integral. Only in the case of a periodic pore space does (2.11) become a discrete matrix eigenvalue problem and thus numerically much more tractable. In that case, all the eigenvalues fall into quasicontinuous bands $\mu_{n\mathbf{q}}, \lambda_{m\mathbf{q}}$ and the eigenfunctions have the Bloch-Floquet form

$$\psi_{n\mathbf{q}}(\mathbf{r}) e^{i\mathbf{q}\cdot\mathbf{r} - \mu_{n\mathbf{q}} t}, \quad \phi_{m\mathbf{q}}(\mathbf{r}) e^{i\mathbf{q}\cdot\mathbf{r} - \lambda_{m\mathbf{q}} t}, \tag{2.15}$$

where n, m are band indices, $\mathbf{q}$ is a wave vector in the first Brillouin zone of reciprocal space, and $\psi_{n\mathbf{q}}(\mathbf{r})$, $\phi_{m\mathbf{q}}(\mathbf{r})$ are periodic with the same kind of periodicity as that of the pore space. As usual, the overlap integral between two Bloch functions with different $\mathbf{q}$ vectors vanishes and (2.9) is replaced by

$$(\mu_{n\mathbf{q}} - \lambda_{m\mathbf{q}}) \int_{V_p \cap V_a} dV \phi_{m\mathbf{q}}^*(\mathbf{r}) \psi_{n\mathbf{q}}(\mathbf{r}) = \rho \oint_{\partial V_p \cap V_a} dS \phi_{m\mathbf{q}}^*(\mathbf{r}) \psi_{n\mathbf{q}}(\mathbf{r}), \tag{2.16}$$

where both the volume and the surface integrations are now restricted to the pore volume or pore-matrix interface within a single unit cell, whose volume is denoted by V_a. This result already appears in Ref. [15], where it was used as the basis of a perturbation expansion for $\psi_{n\mathbf{q}}$. Here we use the discrete nature of the eigenvalue spectrum for a given value of $\mathbf{q}$ in order to get a discrete matrix version of (2.10)–(2.12), namely,

$$\psi_{n\mathbf{q}} = \sum_m A_m^{(n)}(\mathbf{q}) \phi_{m\mathbf{q}}, \tag{2.17}$$

$$(\mu_{n\mathbf{q}} - \lambda_{m\mathbf{q}}) A_m^{(n)}(\mathbf{q}) = \rho \sum_p V_{mp}(\mathbf{q}) A_p^{(n)}(\mathbf{q}), \tag{2.18}$$

$$V_{mp}(\mathbf{q}) \equiv \frac{1}{V_a} \oint_{\partial V_p \cap V_a} dS \phi_{m\mathbf{q}}^*(\mathbf{r}) \phi_{p\mathbf{q}}(\mathbf{r}), \tag{2.19}$$

where $\phi_{m\mathbf{q}}(\mathbf{r})$ are taken to be normalized as

$$\frac{1}{V_a} \int_{V_p \cap V_a} dV \phi_{m\mathbf{q}}^* \phi_{p\mathbf{q}} = \delta_{mp}. \tag{2.20}$$

Note that this normalization differs from the one previously assumed for both ϕ_μ and ψ_μ in (2.3). With the new normalization we get

$$\phi_{00}(\mathbf{r}) = \frac{1}{\sqrt{\phi}}, \tag{2.21}$$

$$V_{00}(\mathbf{0}) = \frac{S_p}{V_p}, \tag{2.22}$$

where $\phi \equiv V_p/V$ is the porosity or fraction of the total volume V occupied by the pore space. The first of these expressions is obviously different from (2.13), but the second one is exactly the same as the result obtained previously for V_{00} [see (2.14)]. The matrix $V_{mp}(\mathbf{q})$ is clearly Hermitian, therefore (2.18) can be solved using standard numerical methods to obtain the eigenvalues $\mu_{n\mathbf{q}}$ and the normalized, mutually orthogonal eigenvectors $A_m^{(n)}(\mathbf{q})$. These eigenvectors can be used in (2.17) to calculate $\psi_{n\mathbf{q}}(\mathbf{r})$, which then have the same orthogonality and normalization properties (2.20) as the $\phi_{m\mathbf{q}}(\mathbf{r})$.

In terms of these eigenstates, G becomes

$$G(\mathbf{r}, \mathbf{r}', t) = \frac{1}{V} \sum_{n,\mathbf{q}} e^{-\mu_{n\mathbf{q}} t} \psi_{n\mathbf{q}}(\mathbf{r}) \psi_{n\mathbf{q}}^*(\mathbf{r}') e^{i\mathbf{q}\cdot(\mathbf{r} - \mathbf{r}')}, \tag{2.23}$$

while M is given by the particularly concise expression

$$M(\mathbf{k}, t) = \frac{1}{\phi} \sum_n e^{-\mu_{n\mathbf{q}} t} |\tilde{\psi}_{n\mathbf{q}}(\mathbf{g_k})|^2 \big|_{\mathbf{q} = \mathbf{k} - \mathbf{g_k}}, \tag{2.24}$$

where

$$\tilde{\psi}_{n\mathbf{q}}(\mathbf{g}) \equiv \frac{1}{V_a} \int_{V_p \cap V_a} dV \psi_{n\mathbf{q}}(\mathbf{r}) e^{-i\mathbf{g}\cdot\mathbf{r}} \tag{2.25}$$

are the Fourier expansion coefficients of $\psi_{n\mathbf{q}}(\mathbf{r})$, $\mathbf{g}$ is a vector of the reciprocal lattice appropriate to the nature of the pore space periodicity, and $\mathbf{g_k}$ is the reciprocal

lattice vector that is closest to $\mathbf{k}$. For small $\mathbf{k}$, i.e., those that are inside the first Brillouin zone, we have $\mathbf{g_k} = \mathbf{0}$ and $\mathbf{q} = \mathbf{k}$.

From numerical computations of $M(\mathbf{k},t)$ at small $\mathbf{k}$ we can deduce the bulk effective, time-dependent, microgeometry restricted diffusion coefficient of the porous medium $D(t)$ using (1.6). For short times t, the values thus obtained can be compared with the explicit asymptotic expressions for $D(t)$ given in Ref. [14], as well as with further expressions derived by us (see Appendix C). At long times only the lowest band of eigenvalues $\mu_{0\mathbf{q}}$ is important for calculating $M(\mathbf{k},t)$, unless the weight $|\tilde{\psi}_{0\mathbf{q}}(\mathbf{g_k})|^2$ happens to be very small. The bulk effective stationary diffusion coefficient D_e is determined from the small $\mathbf{q}$ behavior of $\mu_{0\mathbf{q}}$. For microstructures with cubic point symmetry we have (for lower point symmetries D_e is usually a second rank tensor instead of a scalar quantity)

$$\mu_{0\mathbf{q}} = \mu_{00} + D_e|\mathbf{q}|^2 + O(|\mathbf{q}|^4). \tag{2.26}$$

The $\mathbf{q} = 0$ eigenvalues provide a (discrete) spectrum of relaxation rates for the total magnetization $M(\mathbf{0},t)$

$$M(\mathbf{0},t) = \frac{1}{\phi}\sum_n e^{-\mu_{n0}t}|\tilde{\psi}_{n0}(\mathbf{0})|^2, \tag{2.27}$$

to each of which must be added the intrinsic relaxation rate of nuclear magnetization in the pure pore fluid. Usually even μ_{00}, the lowest of the porous medium rates, is considerably greater than the intrinsic rate. Therefore when a spectrum of total relaxation rates is determined, by an appropriate analysis of a free induction decay NMR or a sequence of spin echo experiments on a fluid filled porous medium, the results are essentially the eigenvalues μ_{n0} weighted by $|\tilde{\psi}_{n0}(\mathbf{0})|^2$.

In practice, the matrix elements $V_{nm}(\mathbf{q})$ are evaluated using the Fourier expansion coefficients of $\phi_{m\mathbf{q}}(\mathbf{r})$

$$V_{nm}(\mathbf{q}) = 4\sum_{\mathbf{g}}\sum_{\mathbf{g}'}\tilde{\phi}^*_{n\mathbf{q}}(\mathbf{g})\,K(\mathbf{g}-\mathbf{g}')\,\tilde{\phi}_{m\mathbf{q}}(\mathbf{g}'), \tag{2.28}$$

where

$$\tilde{\phi}_{n\mathbf{q}}(\mathbf{g}) \equiv \frac{1}{V_a}\int_{V_p\cap V_a} dV\,\phi_{n\mathbf{q}}(\mathbf{r})\,e^{-i\mathbf{g}\cdot\mathbf{r}}, \tag{2.29}$$

$$K(\mathbf{g}) \equiv \frac{1}{V_a}\oint_{\partial V_p\cap V_a} dS\,e^{-i\mathbf{g}\cdot\mathbf{r}}. \tag{2.30}$$

The Fourier expansion coefficients of the $\rho = 0$ eigenfunctions $\tilde{\phi}_{n\mathbf{q}}(\mathbf{g})$, which are needed for evaluating $V_{nm}(\mathbf{q})$, were calculated by solving a discrete matrix version of the eigenvalue problem (2.5) and (2.6), as described in Ref. [16]. A somewhat subtle but important technical point is the factor 4 which appears in (2.28): It arises from the fact that the Fourier series for $\theta_p(\mathbf{r})\phi_{n\mathbf{q}}(\mathbf{r})$ [$\theta_p(\mathbf{r})$ is the characteristic or indicator function of the pore space, equal to 1 inside that space and 0 elsewhere] at the pore-matrix interface, where this function has a jump discontinuity, really converges to 1/2 of the value of $\phi_{n\mathbf{q}}(\mathbf{r})$ at the interface—this is explained in greater detail in Appendix A. The values of $K(\mathbf{g})$ in general depend upon details of the microstructure and periodicity, but $K(\mathbf{0})$ has a general and simple value, namely,

$$K(\mathbf{0}) = \frac{S_p}{V_a} = \phi\frac{S_p}{V_p}. \tag{2.31}$$

We considered a set of samples where a simple cubic array of identical spherical obstacles of radius R, with lattice constant a, is embedded in a uniform fluid medium with diffusion coefficient D_p. Samples with different sphere sizes were considered, including cases where neighboring spheres overlap and cases where they are well separated: Our approach is able to treat periodic samples with both high and low porosities.

Two important microstructural parameters of this system are the porosity ϕ and the surface-to-volume ratio S_p/V_p of the pore space. In terms of the sphere-radius-to-unit-cell-edge ratio $x \equiv R/a$, these parameters are given by

$$\phi = \begin{cases} 1-\frac{4\pi}{3}x^3 & \text{for } 0 \le x \le \frac{1}{2} \\ & \text{(non-overlapping obstacles)} \\ 1+\frac{\pi}{4}-3\pi x^2+\frac{8\pi}{3}x^3 & \text{for } \frac{1}{2} \le x \le \frac{1}{\sqrt{2}} \\ & \text{(overlapping obstacles),} \end{cases} \tag{2.32}$$

$$\frac{aS_p}{V_p} = \begin{cases} \dfrac{4\pi x^2}{1-\frac{4\pi}{3}x^3} & \text{for } 0 \le x \le \frac{1}{2} \\ \dfrac{2\pi x(3-4x)}{1+\frac{\pi}{4}-3\pi x^2+\frac{8\pi}{3}x^3} & \text{for } \frac{1}{2} \le x \le \frac{1}{\sqrt{2}}. \end{cases} \tag{2.33}$$

When $x > 1/\sqrt{2}$, the overlapping spherical obstacles are so large that the pore space becomes a set of isolated, unconnected pockets. Such a collection of unconnected pores was considered in Refs. [8,9]. Here we limit our discussion to the case $x < 1/\sqrt{2}$, when all the pore space is connected.

Because of the simple nature of the pore-matrix interface in the nonoverlapping case, when $x < 1/2$ (i.e., in a single unit cell it is just the total surface area of a single spherical obstacle), a closed form expression is easily obtained for $K(\mathbf{g})$

$$K(\mathbf{g}) = \frac{4\pi R^2}{a^3}\,\frac{\sin(|\mathbf{g}|R)}{|\mathbf{g}|R} = \phi\frac{S_p}{V_p}\,\frac{\sin(|\mathbf{g}|R)}{|\mathbf{g}|R} \quad \text{for } x \le \frac{1}{2}. \tag{2.34}$$

When $\frac{1}{2} < x \le \frac{1}{\sqrt{2}}$, the pore-matrix interface is composed of the surface of a spherical obstacle out of which six circular sections have been cut out due to overlaps with neighboring obstacles. For those cases, $K(\mathbf{g})$ was evaluated by numerical integration of (2.30) over the interface.

The $\mathbf{g}$ vectors also form a simple cubic lattice and are given by

$$\mathbf{g} = \frac{2\pi}{a}(n_x, n_y, n_z), \tag{2.35}$$

n_x, n_y, n_z are integers. In order to get a finite matrix eigenvalue problem for $\lambda_{n\mathbf{q}}, \tilde{\phi}_{n\mathbf{q}}(\mathbf{g})$, we included $\mathbf{g}$ vectors with integer components n_x, n_y, n_z running from $-N$ to N. The total number of $\mathbf{g}$ vectors is thus $(2N+1)^3$, which translates into a $(2N+1)^3 \times (2N+1)^3$ matrix eigenvalue problem for the $\rho = 0$ eigenstates. That problem must be solved carefully, using the method of Ref. [16] in order to avoid singularities which arise from the treatment of the boundary condition at the pore-matrix interface. After all of the $\rho = 0$ eigenstates are found [their total number in this calculation is, of course, $(2N+1)^3$], the eigenvectors $\tilde{\phi}_{n\mathbf{q}}(\mathbf{g})$ are used to construct the $\hat{V}(\mathbf{q})$ matrix using (2.28). That matrix is also of size $(2N+1)^3 \times (2N+1)^3$ and is used in (2.18), along with the $\rho = 0$ eigenvalues, to construct the matrix for the $\rho \neq 0$ eigenvalue problem. After that is solved, the eigenvectors $A_m^{(n)}(\mathbf{q})$ are used to calculate the Fourier coefficients $\tilde{\psi}_{n\mathbf{q}}(\mathbf{g})$ by

$$\tilde{\psi}_{n\mathbf{q}}(\mathbf{g}) = \sum_m A_m^{(n)}(\mathbf{q}) \tilde{\phi}_{m\mathbf{q}}(\mathbf{g}) \tag{2.36}$$

and those are then used, along with the eigenvalues $\mu_{n\mathbf{q}}$, to calculate $G(\mathbf{r}, \mathbf{r}', t)$ and $M(\mathbf{k}, t)$ from (2.23) and (2.24).

It should be noted that because the eigenvalues of the diffusion problem are only bounded (by 0) from below, large eigenvalues can never be calculated with any precision by using a finite, truncated matrix representation. However, if t is not too short, then only the low lying eigenstates are needed for an accurate calculation of measurable quantities such as $G(\mathbf{r}, \mathbf{r}', t)$, $M(\mathbf{k}, t)$, and $D(t)$. Furthermore, for sufficiently short times closed form asymptotic evaluations of the Laplace transform of $G(\mathbf{r}, \mathbf{r}', t)$ lead to explicit expressions for all of the above quantities in the case when $(D_p t)^{1/2} S_p/V_p \ll 1$ and $\rho(t/D_p)^{1/2}$ is either very small or very large compared to 1 (see Ref. [14] and Appendix C).

Finally, it should be noted that many of the $\rho = 0$ eigenstates are spurious and appear as a result of the incorporation of the boundary condition (2.6) into the differential equation for the chemical potential [16]. They did not cause much trouble because the Fourier coefficients $\tilde{\phi}_{n\mathbf{q}}(\mathbf{g})$ associated with the low lying spurious states are very small. Nevertheless, in some of the previous $\rho = 0$ calculations we found that it was necessary to discard those spurious eigenstates which had eigenvalues below the lowest band of true eigenvalues $\lambda_{0\mathbf{q}}$ in order to get accurate results near $\mathbf{k}$ values where $M(\mathbf{k}, t)$ had a minimum [17]. The low lying spurious states that were discarded were identified by the fact that their norm

$$\sum_{\mathbf{g}} |\tilde{\phi}_{n\mathbf{q}}(\mathbf{g})|^2 \tag{2.37}$$

is very small, in contrast to the norm of the low lying true eigenstates which is close to 1.

In view of this experience, although all of the $\rho = 0$ eigenstates were used in constructing the $\hat{V}(\mathbf{q})$ matrix, including the spurious ones, we again monitored the norm of the $\rho \neq 0$ eigenstates

$$\sum_{\mathbf{g}} |\tilde{\psi}_{n\mathbf{q}}(\mathbf{g})|^2 \tag{2.38}$$

and found that the low lying eigenstates clearly fall into two groups. In one group this norm is close to 1, indicating the states to be true eigenstates. In the other group the norm is very small, and those states were then discarded if their eigenvalue was also below the lowest band of true eigenstates.

III. RESULTS

Although all of our results can be expressed in terms of dimensionless parameters, some of them are quoted with physical dimensions. This is done in order to facilitate a comparison with real porous media such as brine saturated porous rock. For this reason we used $D_p = 2.5 \times 10^{-5}$ cm^2/sec, which is the self-diffusion coefficient in water, and a unit cell edge $a = 10$ μm. This results in a characteristic diffusion time scale of $\tau_a \equiv a^2/D_p = 40$ msec. The dimensionless surface absorption parameter is $\rho a/D_p$ and therefore its magnitude is determined not only by the intrinsic absorption rate ρ, but also by a and D_p. In sandstones one typically finds that ρ is in the range 0.003–0.03 cm/sec, while the mean pore diameter is in the range 15–150 μm [6]. Using the extreme values of the mean pore size for a and the extreme values quoted for ρ, we find that $\rho a/D_p = 0.2$–20. This range spans the transition region from weak to strong surface absorption. In view of this observation, we performed calculations for a variety of surface relaxivities which cover both weak and strong absorption, from $\rho a/D_p = 0.1$ up to $\rho a/D_p = 100$.

In actual calculations we used values of N up to 5, in which case the total number of eigenstates is $(2N+1)^3 = 11^3 = 1331$, because for $N = 6$ the number of eigenstates

TABLE I. Results for computed eigenvalues of a simple cubic array of identical touching spheres with porosity ϕ=0.4764 and an interface absorption strength of $\rho a/D_p$=1, where $\mu_{n\mathbf{q}}/D_p = A_n/a^2 + B_n q^2 + O(q^4)$ and the size of the reciprocal lattice varies from N=2 to 5. The values of A_n and B_n are calculated from the computed results for $\mathbf{q}a$=(0.05,0,0) and (0.1,0,0). Note that the coefficient A_0 (i.e., the lowest eigenvalue at q=0) can be compared with the result of perturbation theory $\tau_a \rho S_p/V_p$ (6.5944 in this case; see also Table IV). The coefficient B_0 should be equal to D_e/D_p. The corresponding value for ρ=0 is 0.722.

N	$\mu_{0\mathbf{q}}$	$\mu_{1\mathbf{q}}$	$\mu_{2\mathbf{q}}$	$\mu_{3\mathbf{q}}$	$\mu_{4\mathbf{q}}$	$\mu_{5\mathbf{q}}$	$\mu_{6\mathbf{q}}$
	A_0	A_1	A_2	A_3	A_4	A_5	A_6
2	6.474	39.96	47.70	74.84	97.98	107.45	141.17
3	6.114	39.32	47.26	74.75	100.93	107.55	145.49
4	6.041	39.32	47.05	74.98	102.16	107.40	148.05
5	5.984	39.22	46.95	75.07	102.78	107.31	149.62
	B_0	B_1	B_2	B_3	B_4	B_5	B_6
2	0.689	-9.932	9.908	1.757	-1.549	0.320	3.773
3	0.687	-9.572	9.612	1.619	-4.093	1.707	3.067
4	0.683	-9.849	9.937	1.505	-3.413	2.720	2.640
5	0.682	-9.843	9.964	1.437	-3.987	3.400	2.280

TABLE II. Computed results of some selected elements of $\tilde{\psi}_{n\mathbf{q}}(\mathbf{g})$ for the three lowest eigenvalues with non-negligible weights, denoted by $\mu_{0\mathbf{q}}, \mu_{1\mathbf{q}}, \mu_{2\mathbf{q}}$, for a simple cubic array of identical touching spheres with ϕ=0.476 and $\mathbf{q}a$=(0.1,0,0) for the cases $\rho a/D_p$=1 and $\rho a/D_p$=10. The $\mathbf{g}$ vectors appearing in this table are denoted by a triplet of integers n_x, n_y, n_z, where $\mathbf{g} = \frac{2\pi}{a}(n_x, n_y, n_z)$; e.g., $\tilde{\psi}_{1\mathbf{q}}(000)$ is the same as $\tilde{\psi}_{1\mathbf{q}}(\mathbf{0})$. The reciprocal lattice used varies in size from $N = 2$ up to $N = 5$.

N	$\mu_{0\mathbf{q}}$		$\mu_{1\mathbf{q}}$		$\mu_{2\mathbf{q}}$	
	$\rho a/D_p$=1	$\rho a/D_p$=10	$\rho a/D_p$=1	$\rho a/D_p$=10	$\rho a/D_p$=1	$\rho a/D_p$=10
	$\lvert\tilde{\psi}_{0\mathbf{q}}(000)\rvert^2$	$\lvert\tilde{\psi}_{0\mathbf{q}}(000)\rvert^2$	$\lvert\tilde{\psi}_{1\mathbf{q}}(000)\rvert^2$	$\lvert\tilde{\psi}_{1\mathbf{q}}(000)\rvert^2$	$\lvert\tilde{\psi}_{2\mathbf{q}}(000)\rvert^2$	$\lvert\tilde{\psi}_{2\mathbf{q}}(000)\rvert^2$
2	0.4731	0.3663	0.67×10^{-6}	0.16×10^{-3}	0.36×10^{-4}	0.25×10^{-4}
3	0.4735	0.3832	0.64×10^{-6}	0.29×10^{-4}	0.35×10^{-4}	0.14×10^{-3}
4	0.4734	0.3900	0.68×10^{-6}	0.19×10^{-4}	0.36×10^{-4}	0.15×10^{-3}
5	0.4734	0.3927	0.68×10^{-6}	0.12×10^{-4}	0.36×10^{-4}	0.15×10^{-3}
	$\lvert\tilde{\psi}_{0\mathbf{q}}(100)\rvert^2$	$\lvert\tilde{\psi}_{0\mathbf{q}}(100)\rvert^2$	$\lvert\tilde{\psi}_{1\mathbf{q}}(100)\rvert^2$	$\lvert\tilde{\psi}_{1\mathbf{q}}(100)\rvert^2$	$\lvert\tilde{\psi}_{2\mathbf{q}}(100)\rvert^2$	$\lvert\tilde{\psi}_{2\mathbf{q}}(100)\rvert^2$
2	0.05720	0.07814	0.1280	0.05673	0.2523	0.2417
3	0.05731	0.07766	0.1283	0.02922	0.2508	0.2766
4	0.05741	0.07714	0.1270	0.04498	0.2520	0.2665
5	0.05748	0.07646	0.1268	0.06066	0.2522	0.2539
	$\lvert\tilde{\psi}_{0\mathbf{q}}(200)\rvert^2$	$\lvert\tilde{\psi}_{0\mathbf{q}}(200)\rvert^2$	$\lvert\tilde{\psi}_{1\mathbf{q}}(200)\rvert^2$	$\lvert\tilde{\psi}_{1\mathbf{q}}(200)\rvert^2$	$\lvert\tilde{\psi}_{2\mathbf{q}}(200)\rvert^2$	$\lvert\tilde{\psi}_{2\mathbf{q}}(200)\rvert^2$
2	0.00333	0.00375	0.01625	0.00173	0.01252	0.02466
3	0.00331	0.00407	0.01523	0.00593	0.01226	0.02164
4	0.00327	0.00405	0.01502	0.00783	0.01245	0.02014
5	0.00326	0.00403	0.01484	0.00931	0.01248	0.01840

($13^3 = 2197$) becomes too large to evaluate without invoking special measures. We performed a number of tests for convergence of our results in the various stages of calculation. For the $\rho = 0$ eigenstate calculation those are described in Refs. [16,17] along with all the other details. In addition to those, we tested several eigenvalues $\mu_{n\mathbf{q}}$ for convergence with increasing N (see Table I for a demonstration of such a test) and also the results for the Fourier coefficients $\tilde{\psi}_{n\mathbf{q}}(\mathbf{g})$, the eigenvectors $A_m^{(n)}(\mathbf{q})$, and the matrix elements $V_{mn}(\mathbf{q})$ (see Tables II and III). We also tested the final results for $D(t)$ and $M(\mathbf{k}, t)$ for convergence with increasing N [see Fig. 1(a), where $D(t)$ is plotted at short times for different values of N].

We compared our numerical results for $D(t)$ to the approximate short time asymptotic expressions of Ref. [14] [see Figs. 1(b) and 1(c)], which are valid when $\rho t \ll (D_p t)^{1/2} \ll a$. Our conclusion from these comparisons is that for small or intermediate values of ρ, namely, $\rho a/D_p \leq 1$, the numerical evaluations of G, M, and $D(t)$ are accurate down to times t which are short enough so that the short time asymptotics can also be used there. Furthermore, it is always sufficient to use $N = 4$ when truncating the reciprocal lattice of $\mathbf{g}$ vectors. For large values of ρ, namely, $\rho a/D_p > 1$, there is a range of intermediate times where both our calculations and the above mentioned short time asymptotics are invalid [see Fig. 1(c)]. In that domain the numerical results are improved by increasing N up to 5. Presumably a further increase would improve their accuracy even more, especially when $\rho a/D_p \gg 1$. Alternatively, it seems that simple interpolation can be used to provide reliable results in the intermediate range of times [see Fig. 1(c)]. In that domain, one can also try to use an asymptotic short time approximation which is valid when $(D_p t)^{1/2} \ll \rho t$. In Ref. [14] an approximation of this type was obtained for a *general microstructure* only when $\rho = \infty$. In Appendix C, we extend this approach to obtain an asymptotic expression for $D(t)$ in a porous

TABLE III. Results for computed eigenvector component $A_0^{(0)}(\mathbf{q})$ at $\mathbf{q}a$=(0.1,0,0) for $\rho a/D_p$=1, 10, and 100 for a simple cubic array of identical touching spheres with porosity ϕ=0.4764 and the size of the reciprocal lattice varying between N=2 and 5. Also shown are the results of the computed matrix elements $V_{00}(\mathbf{q})$, $V_{11}(\mathbf{q})$, and $V_{22}(\mathbf{q})$. Note that the numerically computed value of $V_{00}(\mathbf{q})$ for N=5 is within 1% of the exact value of $V_{00}(\mathbf{0})$ for this microgeometry, i.e., aS_p/V_p=6.5944.

N	$A_0^{(0)}(\rho a/D_p = 1)$	$A_0^{(0)}(\rho a/D_p = 10)$	$A_0^{(0)}(\rho a/D_p = 100)$	aV_{00}	aV_{11}	aV_{22}
2	0.9967	0.8766	0.6023	6.9649	8.5946	7.8542
3	0.9960	0.8960	0.6928	6.6455	8.2669	7.8255
4	0.9969	0.9049	0.7236	6.6490	8.4196	7.7191
5	0.9969	0.9081	0.7400	6.6419	8.4156	7.6906

medium with a general microstructure and large but finite values of ρ, in the regime where $(D_p t)^{1/2} \ll \rho t \ll a$ [see (C13)]. However, we were not able to include the effects of finite radii of curvature of the interface, even for $\rho = \infty$. The values resulting from (C13) are also shown in Fig. 1(c) and they are evidently insufficient to bridge the window of times where our computations, as well as the small ρ approximations, fail.

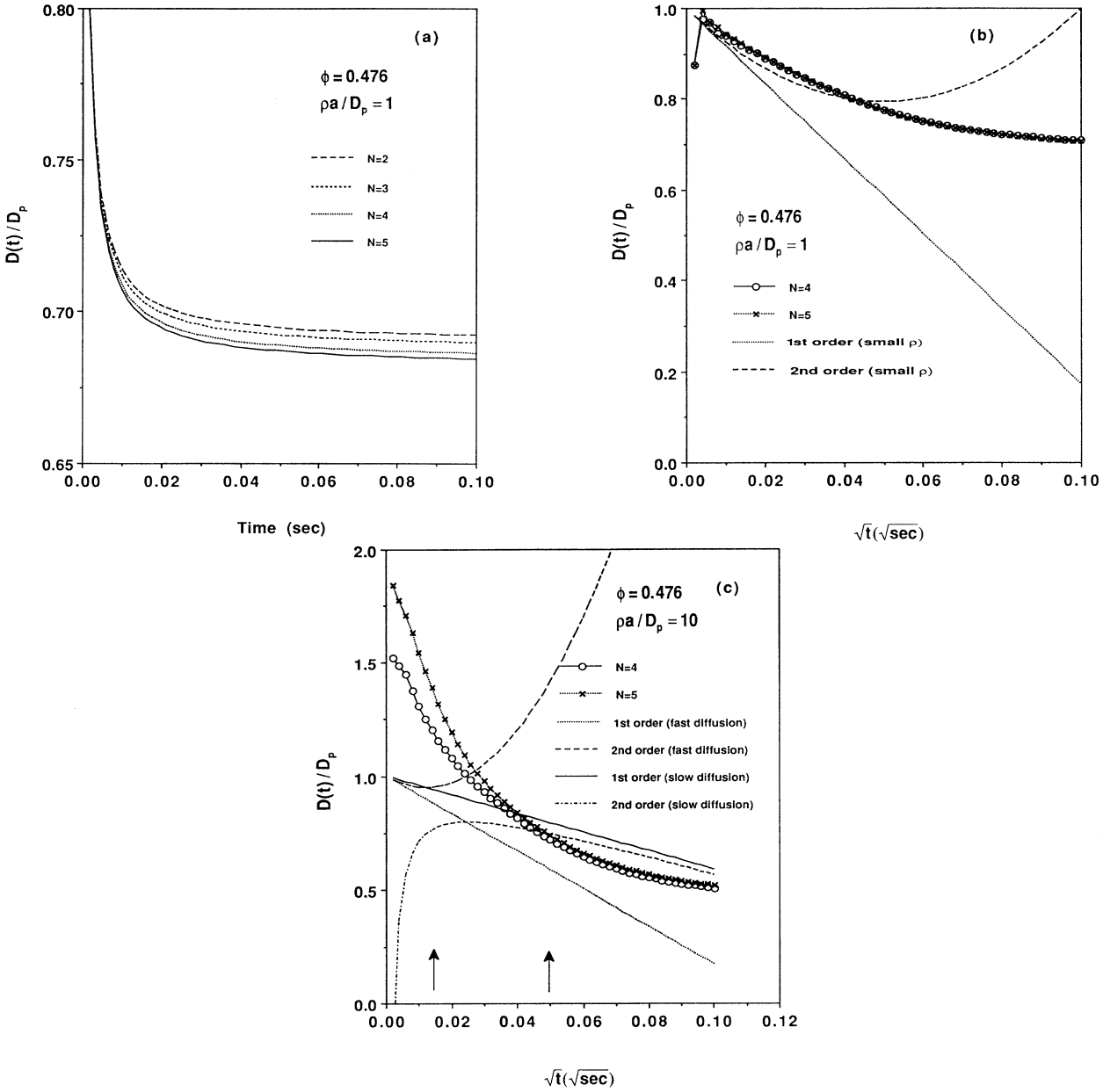

FIG. 1. (a) Results for the bulk effective time-dependent diffusion coefficient $D(t)/D_p$ vs time, in seconds, for a simple cubic array of identical touching spheres ($\phi = 0.4764$), unit cell edge $a = 10\,\mu$m, fluid self-diffusion coefficient $D_p = 2.5\times10^{-5}$ cm^2/sec, and dimensionless interface absorption coefficient $\rho a/D_p = 1$. The size of the reciprocal lattice used for the Fourier expansion varies from N=1 to 5, illustrating the convergence of the computation. (b) Results for $D(t)/D_p$ vs $\sqrt{t}$ for the same sample. Also plotted are the short time asymptotic approximations of Ref. [14] for the *small* ρ *regime*, where $\rho t \ll (D_p t)^{1/2} \ll a$. The first-order asymptotics contain only the term of order $(D_p t)^{1/2} S_p/V_p$, while the second-order asymptotics also contain terms proportional to ρ and to the inverse radii of curvature of the interface [see Eqs. (29) and (39) of Ref. [14]]. (c) Same as (b), but with a higher value of ρ, namely, $\rho a/D_p = 10$. In addition to the above mentioned asymptotic approximations of Ref. [14], we also plot the asymptotic approximations for the *large* ρ *regime*, where $(D_p t)^{1/2} \ll \rho t \ll a$, as obtained in Appendix C [see (C13)]. In this case the first-order asymptotics again contain only the term of order $(D_p t)^{1/2} S_p/V_p$ from (C13), while the second-order asymptotics use *all the terms* in that expression. Vertical arrows mark the time interval where both our numerical computations and the small ρ asymptotic expressions from Ref. [14] are invalid.

In Fig. 2 we show the low lying bands of true (as opposed to spurious) reduced (dimensionless) eigenvalues $\tilde{\mu}_{n\mathbf{q}} \equiv \mu_{n\mathbf{q}}\tau_a$ for $\mathbf{q}$ in the (100) direction, when $\rho a/D_p = 1$ and 10. This figure can be compared with a similar one for the $\rho = 0$ case, which appears as Fig. 2 in Ref. [17]. Values of $|\mathbf{q}|a$ are shown beyond the upper edge of the first Brillouin zone at $|\mathbf{q}|a = \pi$ in order to emphasize the periodic nature of $\mu_{n\mathbf{q}}$ in the extended zone scheme. Note that when $\rho a/D_p$ is increased from 0 to 1 the detailed band structure changes only slightly, apart from a general displacement upwards, but when $\rho a/D_p = 10$, many details of the band structure change appreciably.

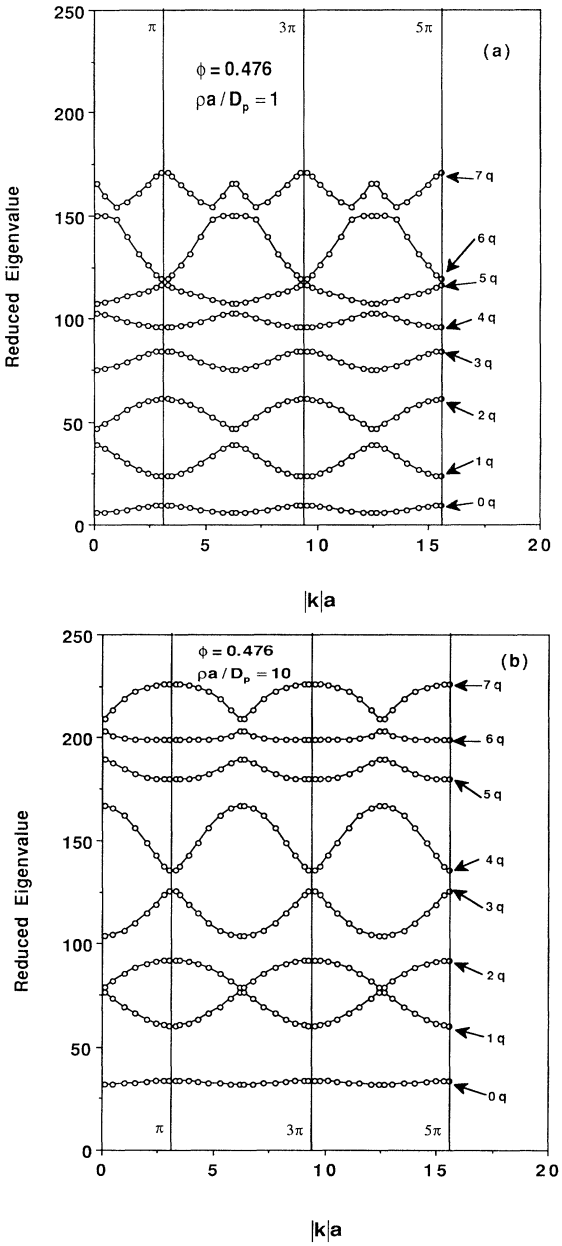

FIG. 2. Results for the seven lowest reduced true eigenvalues $\tilde{\mu}_{n\mathbf{k}} \equiv \mu_{n\mathbf{k}}\tau_a$ as functions of $|\mathbf{k}|a$ along the (100) direction in the one-dimensional extended zone scheme for a simple cubic array of identical touching spheres (ϕ=0.4764) (a) for $\rho a/D_p = 1$ and (b) for $\rho a/D_p = 10$. The bands identified as $0\mathbf{q}$, $1\mathbf{q}$, etc. correspond to the eigenvalues $\mu_{0\mathbf{q}}$, $\mu_{1\mathbf{q}}$, etc. which are exhibited in Tables I and II.

In Tables IV and V we list the values of $\mu_{0\mathbf{q}}$ (i.e., the lowest band of true eigenvalues) for a small value of $\mathbf{q}$, so that they are approximately equal to μ_{00}, which we found at the different porosities and different values of ρ that were considered. Note that calculating $\mu_{0\mathbf{q}}$ exactly at $\mathbf{q} = \mathbf{0}$ would be less accurate because, in this more symmetric point of $\mathbf{q}$ space, there is greater degeneracy among different eigenstates; see Ref. [17]. When both $\rho a/D_p = 0.1$ and $|\mathbf{q}|a = 0.1$, we would expect that $\tilde{\mu}_{0\mathbf{q}} \approx \tilde{\mu}_{00} \approx \tau_a\rho S_p/V_p$. Table V shows that this expectation is well satisfied for the three intermediate values of ϕ, but less so for the two extreme values. In the high porosity case $\phi = 0.700$, we were able to determine the reason for this by comparing our numerical evaluation of $V_{00}(\mathbf{0})$ with an evaluation in which the *exact values* of $\tilde{\phi}_{00}(\mathbf{g})$ [see Eq. (2.57) in Ref. [17]] were used in (2.28). When the sums over reciprocal lattice vectors were similarly restricted, the two calculations led to results that were very close to each other, but the convergence with increasing N was very slow. Consequently even the exact calculation led to substantial deviations from the expected value unless N was assigned extremely large values. This may be connected to the fact that a Fourier expansion was used to represent a discontinuous function (see Appendix A). In the low porosity case $\phi = 0.104$, we were unable to determine the cause of the discrepancy between $\tilde{\mu}_{n\mathbf{q}}$ and $\tau_a\rho S_p/V_p$. We think it is due either to slow convergence of the above mentioned sums in (2.28) or to the fact that both $\theta_{\mathbf{g}}$ and $K(\mathbf{g})$ were calculated by using two-dimensional numerical integration over the interface, with the attendant inaccuracies.

Using the values of $\tilde{\mu}_{00}$ (taken to be approximately equal to $\tilde{\mu}_{0\mathbf{q}}$ of Table IV), we find that the additional spin relaxation rates $\mu_{00} = \tilde{\mu}_{00}/\tau_a$ are in the range 1/60–1/0.8 msec^{-1}. This is well within the range of relaxation rates

TABLE IV. Computed results at N=5 for $A_0^{(0)}(\mathbf{q})$ and the lowest reduced eigenvalue $\tilde{\mu}_{0\mathbf{q}} = \tau_a\mu_{0\mathbf{q}}$ at $\mathbf{q}a$=(0.1,0,0), as compared with the dimensionless parameters $\tau_a\rho V_{00}$ and $\tau_a\rho S_p/V_p$ at various interfacial absorption strengths for a simple cubic array of identical touching spheres with porosity ϕ=0.4764. Note that the perturbation result $\tilde{\mu}_{00} = \tau_a\rho V_{00}$ is still within 10% of the exact answer when $\rho a/D_p$=1 and that even when $\rho a/D_p$=10, $A_0^{(0)}(\mathbf{q})$ is only 10% away from the perturbation result $A_0^{(0)}(\mathbf{q}) = 1$. Also shown are the values of the bulk effective stationary or long time diffusion coefficient D_e/D_p, obtained from the q^2 term in $\tilde{\mu}_{0\mathbf{q}}$.

$\rho a/D_p$	$A_0^{(0)}(\mathbf{q})$	$\tilde{\mu}_{0\mathbf{q}}$	$\tau_a\rho V_{00}$	$\tau_a\rho S_p/V_p$	D_e/D_p
0.1	1.0000	0.6642	0.6642	0.6594	0.716
1	0.9969	5.9912	6.6419	6.5944	0.681
10	0.9081	31.0305	66.4194	65.9444	0.433
30	0.8097	43.9898	199.2582	197.8333	0.266
100	0.7400	51.0244	664.1941	659.4443	0.182

TABLE V. Computed lowest eigenvalue $\tilde{\mu}_{0\mathbf{q}}$ (in dimensionless form) at $\mathbf{q}a=(0.1,0,0)$ as compared with $\tau_a\rho S_p/V_p$ for simple cubic arrays of nonverlapping, touching, and overlapping spheres with different porosities and different ρ. The reciprocal lattice size was $N = 5$.

$\rho a/D_p$	0.1		1		10		100	
ϕ	$\tilde{\mu}_{0\mathbf{q}}$	$\tau_a\rho S_p/V_p$	$\tilde{\mu}_{0\mathbf{q}}$	$\tau_a\rho S_p/V_p$	$\tilde{\mu}_{0\mathbf{q}}$	$\tau_a\rho S_p/V_p$	$\tilde{\mu}_{0\mathbf{q}}$	$\tau_a\rho S_p/V_p$
0.700	0.3365	0.3096	3.0647	3.0960	17.062	30.960	28.401	309.60
0.476	0.6642	0.6594	5.9912	6.5944	31.031	65.944	51.024	659.44
0.328	0.8528	0.8424	7.9099	8.4235	43.624	84.235	73.170	842.35
0.202	1.1113	1.1198	10.4464	11.1978	60.746	111.978	106.851	1119.78
0.104	1.4817	1.5708	13.8959	15.7080	85.830	157.080	170.730	1570.80

observed in NMR experiments on protons in a variety of brine saturated natural sandstones (see Ref. [6]).

In Table IV we also show the values of $A_0^{(0)}$, ρV_{00}, $\rho S_p/V_p$, and D_e/D_p [D_e is the bulk effective value or long time limit of $D(t)$] for various values of $\rho a/D_p$. This table allows us to examine two different questions: (a) How accurate is the numerical computation of the matrix elements $V_{mn}(\mathbf{q})$? (b) How accurate would a perturbation treatment be which calculated everything to leading order in $\rho a/D_p$? In order to answer the first question, we note that column 4 of this table shows numerical results for the particular matrix element $V_{00}(\mathbf{q})$, while column 5 shows the *exact result* for the same quantity. The second question can be answered by seeing how different the numerically computed value of $A_0^{(0)}(\mathbf{q})$ is from 1 and how different the similarly computed value of $\tilde{\mu}_{0\mathbf{q}} \approx \tilde{\mu}_{00}$ is from the first-order perturbation theory value $\tau_a\rho V_{00}$ (see Appendix B). Evidently, even for the medium large value of $\rho a/D_p = 1$, perturbation theory is still a quite good approximation.

In Fig. 3 we plot $D(t)/D_p$ for different porosities and different values of ρ. Note that the value attained by $D(t)$ in the limit $t \to \infty$ is just the bulk effective diffusion coefficient D_e. For the $\rho = 0$ case, this quantity is related to the so-called formation factor F through the relation (see, e.g., Ref. [13])

$$\frac{D_e}{D_p} = \frac{1}{\phi F} = \frac{1}{\phi}\,\frac{\sigma_e}{\sigma_p}, \tag{3.1}$$

where σ_p and σ_e are the electrical conductivity of the pore fluid and the bulk effective conductivity, respectively, and the matrix component is assumed to be a perfect insulator. In contrast to this, when $\rho \neq 0$ the only way to calculate D_e is by using (2.26). In Table VI we show D_e/D_p for various values of ϕ and ρ, including $\rho = 0$. Also shown, for comparison with the $\rho = 0$ values of D_e/D_p, are the values of $1/\phi F$, where F was evaluated using the method of Ref. [18].

In Fig. 4 we show the low lying reduced eigenvalues $\tilde{\mu}_{n\mathbf{q}}$ as functions of $\rho a/D_p$. When $\rho a/D_p \ll 1$, these eigenvalues exhibit the behavior predicted by perturbation theory [see (B1)]

$$\tilde{\mu}_{n\mathbf{q}} - \tilde{\lambda}_{n\mathbf{q}} \propto \rho. \tag{3.2}$$

In particular, the lowest eigenvalue then satisfies [see (B9)]

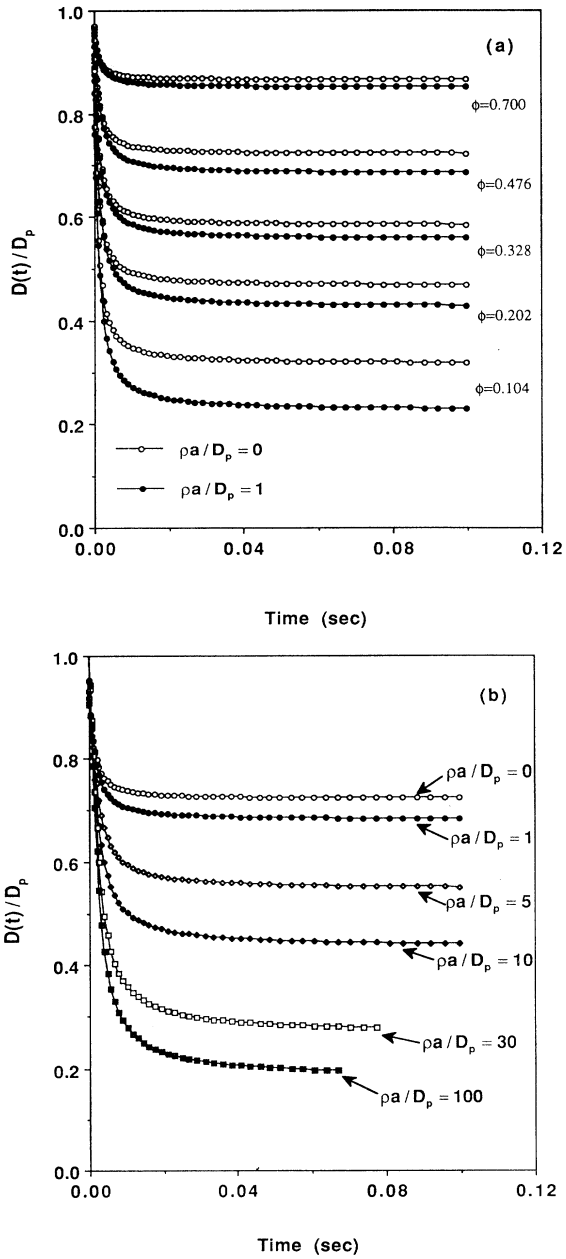

FIG. 3. Bulk effective time-dependent diffusion coefficient $D(t)/D_p$ plotted vs time t (a) for various porosities ϕ and $\rho a/D_p = 1$ and 0 and (b) for touching spheres ($\phi = 0.476$) and various values of $\rho a/D_p$.

$$\tilde{\mu}_{00} = \frac{\rho a}{D_p} \frac{a S_p}{V_p}. \tag{3.3}$$

In order to demonstrate the quality of these calculations, we show some plots of $\tilde{\mu}_{0\mathbf{q}}$ for $\mathbf{q}$ in the (100) direction with $\rho a/D_p = 1$ and $N = 2, \ldots, 5$ (see Fig. 5).

In Fig. 6 we present results for $M(\mathbf{k}, t)$ with $\mathbf{k}$ in the (100) direction at $\rho a/D_p = 1$ and 10, while in Fig. 7 the same results are used to plot the ratio $M(\mathbf{k}, t)/M(\mathbf{0}, t)$, together with $M(\mathbf{k}, t)$ for $\rho = 0$. The purpose of the latter plot is to further study the validity of the finding that, when $\rho a/D_p$ is small, the following relation holds approximately [12]:

$$M(\mathbf{k}, t) \approx M(\mathbf{0}, t) \left[M(\mathbf{k}, t)|_{\rho=0} \right]. \tag{3.4}$$

Figure 7 shows that this finding continues to hold reasonably well up to $\rho a/D_p = 1$. That is why $M(\mathbf{k}, t)$ has the same qualitative appearance as in the $\rho = 0$ case, namely, at long enough times t it develops a series of quasidiffraction peaks whenever $\mathbf{k}$ is equal to a reciprocal lattice vector.

In Fig. 8 we show $M(\mathbf{k}, t)$ and $M(\mathbf{k}, t)/M(\mathbf{0}, t)$ for $\mathbf{k}$ along the (110) direction in a sample of touching spheres at $\rho a/D_p = 1$. The extra minimum which appears for $t \geq 10$ msec at a value of $\mathbf{k}$ that is equal to the reciprocal lattice vector $\mathbf{g} = \frac{2\pi}{a}(110)$ mimics a similar minimum that appeared in the $\rho = 0$ case (see Fig. 11 in Ref. [17]). It is due to the fact that the weight $|\tilde{\psi}_{00}(\mathbf{g})|^2$ is very small for that $\mathbf{g}$, which is very close to a spherical surface in $\mathbf{k}$ space where $\tilde{\psi}_{00}(\mathbf{k}) = 0$.

In Fig. 9 we show $M(\mathbf{k}, t)/M(\mathbf{0}, t)$ for $\mathbf{k}$ along the (100) direction for three different porosities, corresponding to overlapping, nonoverlapping, and just touching spheres, at $\rho a/D_p = 1$. From this figure it is apparent that the behavior of the normalized PFGSE amplitude as function

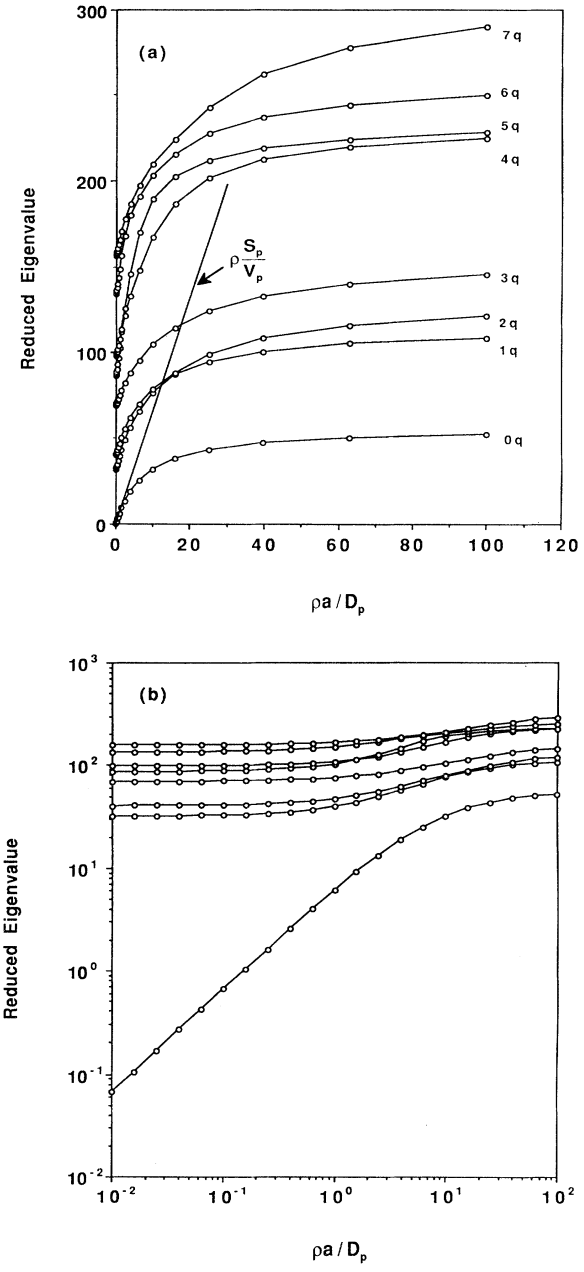

FIG. 4. Low lying reduced true eigenvalues $\tilde{\mu}_{n\mathbf{q}}$ vs $\rho a/D_p$ for $\mathbf{q} = (0.1, 0, 0)$ and $n = 0, 1, \ldots, 7$ (a) in a linear plot and (b) in a log-log plot. This essentially shows the dependence of $\tilde{\mu}_{n\mathbf{0}}$ on ρ, since $|\mathbf{q}|a \ll 2\pi$. Calculating $\tilde{\mu}_{n\mathbf{q}}$ for a small but nonzero value of $\mathbf{q}$ is considerably more accurate than a calculation at $\mathbf{q} = 0$, for reasons which are explained in the text.

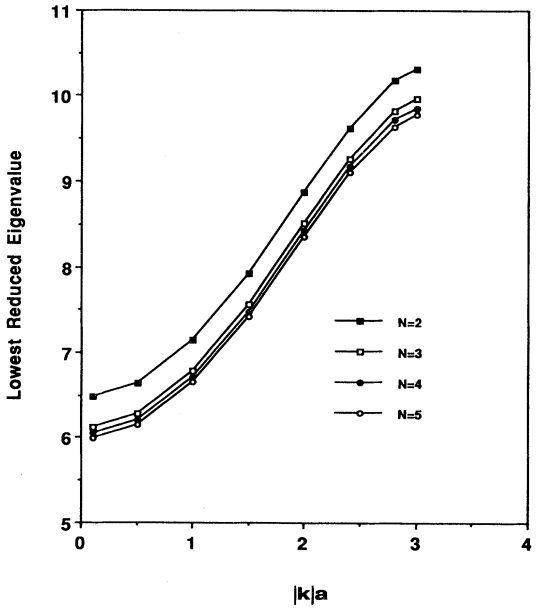

FIG. 5. Plots of the lowest eigenvalue band $\tilde{\mu}_{0\mathbf{k}}$ vs $|\mathbf{k}|a$ for $\mathbf{k}$ in the (100) direction and $N = 2, \ldots, 5$.

TABLE VI. Results at N=5 for the bulk effective stationary diffusion coefficient D_e/D_p for all the values of ρ and ϕ considered. Results at N=4 for nonzero ρ are also shown in parentheses to indicate the convergence. As ρ increases, the convergence gets poorer. For lower porosities, the imprecise calculation of θ_g also leads to poor convergence as discussed in the text. The appearance of ** instead of a numerical entry indicates that the difference between results at N=4 and 5 is greater than 30% and therefore the values obtained are unreliable. The second column shows the values for $\sigma_e/(\phi\sigma_p)$ which were computed using the method of Ref. [18].

	$\rho a/D_p$	D_e/D_p				
ϕ	$\sigma_e/(\phi\sigma_p)$	0	0.1	1	10	100
0.700	0.865	0.865	0.864(0.864)	0.850(0.851)	0.686(0.685)	0.495(0.481)
0.476	0.722	0.722	0.716(0.719)	0.681(0.683)	0.433(0.424)	0.182(0.165)
0.328	0.583	0.582	0.579(0.580)	0.534(0.556)	0.256(0.253)	0.050(0.045)
0.202	0.467	0.466	0.461(0.463)	0.413(0.425)	**	**
0.104	0.315	0.315	0.240(0.303)	**	**	**

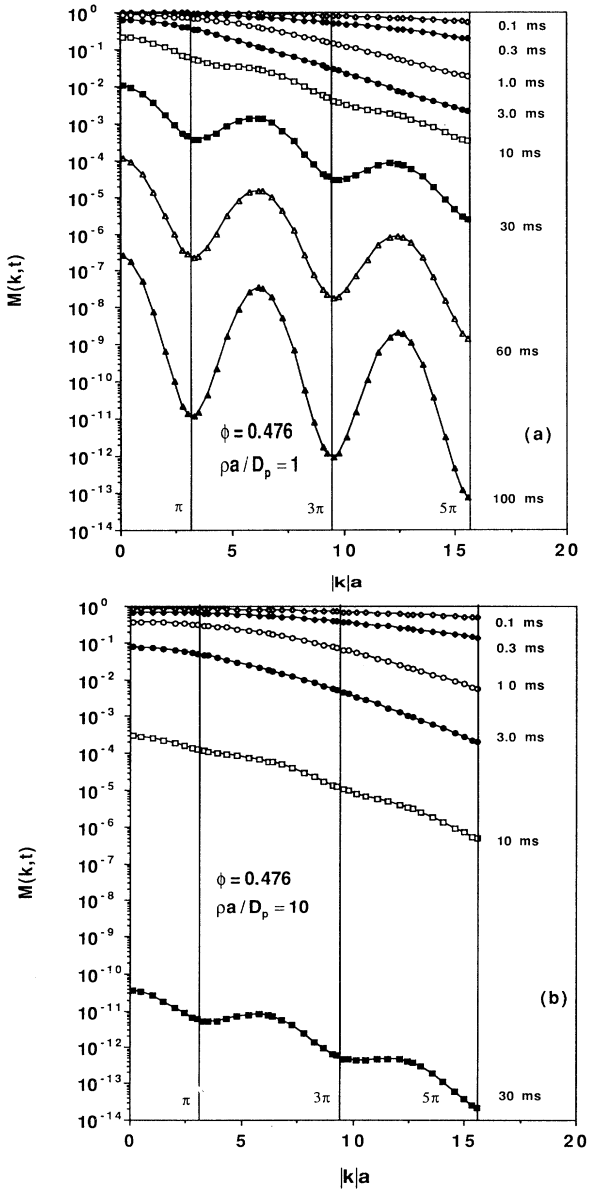

FIG. 6. PFGSE amplitude $M(\mathbf{k},t)$ plotted vs $|\mathbf{k}|a$ along the (100) direction at various times for a cubic array of touching spheres (ϕ = 0.476) (a) for $\rho a/D_p$ = 1 and (b) for $\rho a/D_p = 10$.

of $\mathbf{k}$ is qualitatively similar at the different porosities: The normalized amplitude generally decreases with increasing $|\mathbf{k}|$ in any fixed direction, but when t is large enough there appear quasidiffraction maxima whenever $\mathbf{k}$ equals a reciprocal lattice vector. The general trend of decay with increasing $|\mathbf{k}|$ is weaker the lower the porosity ϕ. This is in agreement with the finding that $D(t)$ decreases with decreasing ϕ at any fixed value of t [see Fig. 3(a)].

IV. DISCUSSION

We presented a method capable of making accurate determinations of all aspects of self-diffusion in a periodic

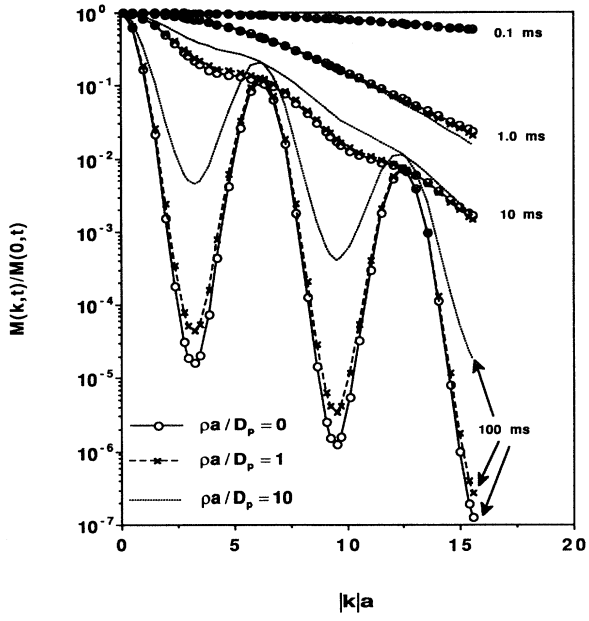

FIG. 7. Plot of the ratio $M(\mathbf{k},t)/M(\mathbf{0},t)$ for the same samples as in Fig. 6, along with results for ρ = 0. Evidently, for $\rho a/D_p \leq 1$, (3.4) is a good approximation, but for $\rho a/D_p = 10$ it is not.

porous medium with nonzero surface absorption. This approach was applied to a set of samples of simple cubic arrays of spherical obstacles, with both high and low porosities and with both weak and strong absorption parameters. A number of measurable macroscopic quantities were calculated, including the macroscopic time-dependent diffusion coefficient and the PFGSE amplitude. These may be compared with results of NMR experiments which would have to be done on synthetically constructed periodic porous media.

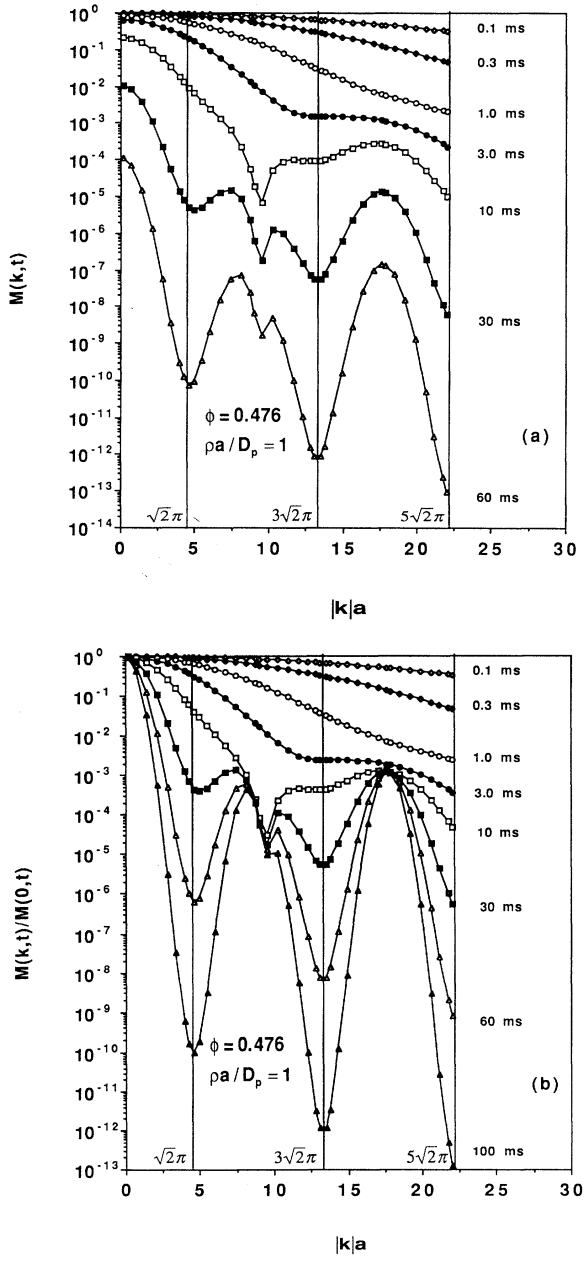

FIG. 8. Plots of (a) $M(\mathbf{k},t)$ and (b) $M(\mathbf{k},t)/M(\mathbf{0},t)$ vs $|\mathbf{k}|a$ along the (110) direction at various times for a cubic array of touching spheres ($\phi = 0.476$) and $\rho a/D_p = 1$.

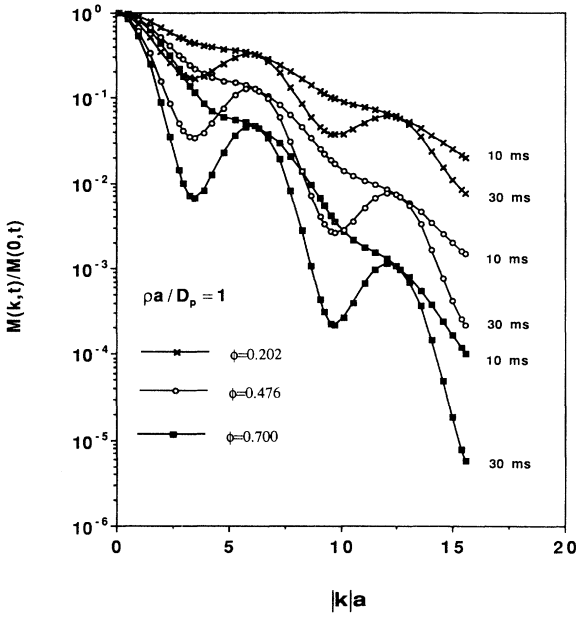

FIG. 9. Plots of $M(\mathbf{k},t)/M(\mathbf{0},t)$ vs $|\mathbf{k}|a$ along the (100) direction for $\rho a/D_p$=1 at various times, for a cubic array of spheres with different values of the porosity ϕ: 0.202 (R/a = 0.575, overlapping spheres), 0.476 (R/a = 0.5, touching spheres), and 0.700 (R/a = 0.415, nonoverlapping spheres).

Among the many results that we presented for the special system of a cubic array of spherical obstacles, we would like to note (a) the values of D_e/D_p for $\rho \neq 0$, (b) the finding that D_e *decreases* with decreasing ϕ and increasing ρ, and (c) the finding that $M(\mathbf{k},t) \approx M(\mathbf{0},t)[M(\mathbf{k},t)|_{\rho=0}]$ up to $\rho a/D_p = 1$.

An even more interesting application of this method would be for the study of diffusion in periodic porous media with a more complicated microstructure, including large pores interconnected by long, narrow tubes. Our approach is not expected to be more difficult to apply to such systems because the main impediment to rapid convergence of our calculations with increasing N seems to be the fact that we are attempting to represent the discontinuous step function $\theta_p(\mathbf{r})$ by a truncated Fourier series, not the complexity of the microgeometry. We believe that such structures can closely mimic the macroscopic properties of many kinds of disordered porous media that are found in nature. Indeed, the values we used for the parameters a, ρ, D_p are all attained in typical brine saturated natural porous rocks and some NMR measurements of $D(t)$ have recently been published [19]. Therefore, as soon as calculations are performed for more realistic microstructures and as good measurements become available of $D(t)$ and $M(\mathbf{k},t)$ in real rocks, we should be able to make some direct comparisons of measurements and calculations.

It should be noted that for porosities lower than $\phi = 0.4764$, when neighboring spherical obstacles have a fi-

nite overlap, we used a two-dimensional numerical integration procedure for computing the Fourier coefficients $\theta_{\mathbf{g}}$ of the characteristic step function $\theta_p(\mathbf{r})$ of the pore space. Those coefficients are used in the initial stage of the calculations, when the $\rho = 0$ eigenstates are computed. This numerical integration introduces computational errors which propagate to the $\rho \neq 0$ eigenstates and may become prohibitively large when ρ is very large. These errors can be avoided by using the infinite series or one-dimensional integral expressions that were developed in Ref. [20] in order to evaluate $\theta_{\mathbf{g}}$ for an array of overlapping spheres. When considering models with a more complicated microstructure, it will probably be computationally advantageous to assume that the pore-matrix interface is composed of a finite set of intersecting planes. This will reduce the computation of $\theta_{\mathbf{g}}$ to a set of purely algebraic steps, since all the integrations will then be elementary.

Of the other calculational methods that have been developed for studying self-diffusion in a porous medium, only the random walker simulations are able to treat systems with low porosity at times which are not very short [11,12,15]. The random walker method has the advantage of being able to cope with disordered structures as well as periodic ones, but it becomes increasingly more difficult and time consuming, and therfore less accurate, as the diffusion time increases. Our method, in contrast, becomes more accurate and easier to use as time increases, especially when $\rho a/D_p \geq 1$ and when ρt is not small compared to $(D_p t)^{1/2}$. A comparative study of the same set of periodic porous samples using the two methods is described in the preceding paper [21].

ACKNOWLEDGMENTS

We wish to thank G.A. LaTorraca for useful discussions and for his comments on this manuscript.

APPENDIX A: DERIVATION OF EQ. (2.28)

In order to understand the origin of the factor 4 which appears in (2.28), we must return to (2.19), namely,

$$V_{mp}(\mathbf{q}) = \frac{1}{V_a} \oint_{\partial V_p \cap V_a} dS \phi^*_{m\mathbf{q}}(\mathbf{r}) \phi_{p\mathbf{q}}(\mathbf{r}). \tag{A1}$$

This is processed by substituting the Fourier series expansion

$$\phi_{p\mathbf{q}}(\mathbf{r}) = \sum_{\mathbf{g}} \tilde{\phi}_{p\mathbf{q}}(\mathbf{g}) e^{i\mathbf{g}\cdot\mathbf{r}} \tag{A2}$$

and a similar expansion for $\phi^*_{m\mathbf{q}}(\mathbf{r})$. A careful inspection of the expression for the coefficients $\tilde{\phi}_{p\mathbf{q}}(\mathbf{g})$, namely [see (2.29)],

$$\tilde{\phi}_{n\mathbf{q}}(\mathbf{g}) = \frac{1}{V_a} \int_{V_p \cap V_a} dV \phi_{n\mathbf{q}}(\mathbf{r}) e^{-i\mathbf{g}\cdot\mathbf{r}}, \tag{A3}$$

reveals that they are actually the Fourier coefficients of the function $\theta_p(\mathbf{r})\phi_{p\mathbf{q}}(\mathbf{r})$, which has a jump discontinuity at the pore-matrix interface and vanishes inside the matrix. The limit value of this function as $\mathbf{r}$ tends to the interface *from inside the pore space* will be denoted by $\phi^{(\mathrm{in})}_{p\mathbf{q}}(\mathbf{r})$—that is the value which should appear in the integrand of (A1). However, the series (A2) converges to $\phi_{p\mathbf{q}}(\mathbf{r})$ for $\mathbf{r}$ inside the pore space, to 0 inside the matrix, and to *one-half of the value of* $\phi^{(\mathrm{in})}_{p\mathbf{q}}(\mathbf{r})$ *at the interface*. Therefore, if we want to use (A2) in (A1), we must compensate for this effect by multiplying each of the Fourier series that are used by a factor 2, resulting in a total factor of 4. This immediately leads to the result

$$\begin{aligned} V_{mp}(\mathbf{q}) &= 4 \sum_{\mathbf{g}} \sum_{\mathbf{g}'} \frac{1}{V_a} \oint_{\partial V_p \cap V_a} dS\, \tilde{\phi}^*_{m\mathbf{q}}(\mathbf{g}) e^{-i\mathbf{g}\cdot\mathbf{r}}\, \tilde{\phi}_{p\mathbf{q}}(\mathbf{g}') e^{i\mathbf{g}'\cdot\mathbf{r}} \\ &= 4 \sum_{\mathbf{g}} \sum_{\mathbf{g}'} \tilde{\phi}^*_{m\mathbf{q}}(\mathbf{g})\, K(\mathbf{g}-\mathbf{g}')\, \tilde{\phi}_{p\mathbf{q}}(\mathbf{g}'), \end{aligned} \tag{A4}$$

where

$$K(\mathbf{g}-\mathbf{g}') = \frac{1}{V_a} \oint_{\partial V_p \cap V_a} dS\, e^{-i(\mathbf{g}-\mathbf{g}')\cdot\mathbf{r}}. \tag{A5}$$

This analysis is corroborated by the fact that the numerical algorithm based upon (A4) yields the correct result for V_{00}, as given in (2.22) (see Table IV).

APPENDIX B: SOME RESULTS FROM PERTURBATION THEORY

For small values of ρ, when $\rho a/D_p \ll 1$, lowest-order perturbation theory can be used to calculate the $\rho \neq 0$ eigenstates from the $\rho = 0$ eigenstates. We do this explicitly for the case of a periodic porous medium, but the same approach can be used even for nonperiodic structures. From (2.18) and (2.19) we thus get for $\mu_{n\mathbf{q}}(\rho)$, recalling the normalization (2.20) of $\phi_{n\mathbf{q}}(\mathbf{r})$ and that of the eigenvectors $A^{(n)}_m(\mathbf{q})$, and assuming that $\mu_{n\mathbf{q}}(0) \equiv \lambda_{n\mathbf{q}}$ is a nondegenerate $\rho = 0$ eigenvalue,

$$\Delta\mu_{n\mathbf{q}} \equiv \mu_{n\mathbf{q}}(\rho) - \mu_{n\mathbf{q}}(0) \approx \rho V_{nn}(\mathbf{q}) = O\left(\frac{\rho}{a}\right), \tag{B1}$$

$$A^{(n)}_m(\mathbf{q}) \approx \frac{\rho V_{nm}(\mathbf{q})}{\lambda_{n\mathbf{q}} - \lambda_{m\mathbf{q}}} = O\left(\frac{\rho a}{D_p}\right), \quad n \neq m \tag{B2}$$

$$|A^{(n)}_n(\mathbf{q})|^2 \approx 1 - O\left(\left(\frac{\rho a}{D_p}\right)^2\right). \tag{B3}$$

The following terms in the perturbation expansions of $\Delta\mu_{n\mathbf{q}}$ and $A^{(n)}_m(\mathbf{q})$, $n \neq m$, are smaller than the leading terms by a factor of order $O(\rho a/D_p) \ll 1$. From these results we can draw some useful conclusions. (a) For small ρ the lowest eigenvalue $\mu_{00}(\rho)$, which vanishes for $\rho = 0$, is given by [see (2.22)]

$$\mu_{00}(\rho) \approx \rho V_{00}(\mathbf{0}) = \rho \frac{S_p}{V_p}. \tag{B4}$$

(b) For small ρ, the decay of magnetization depends only on that eigenvalue: The total magnetization is given by

[see (2.24)]

$$M(\mathbf{0},t)=\frac{1}{\phi}\sum_n e^{-\mu_{n\mathbf{0}}t}|\tilde{\psi}_{n\mathbf{0}}(\mathbf{0})|^2, \tag{B5}$$

and the weights in that expression $[|\tilde{\psi}_{n\mathbf{0}}(\mathbf{0})|^2]$ can be calculated from [see either (2.17) or (2.36)]

$$|\tilde{\psi}_{n\mathbf{q}}(\mathbf{g})|^2=\sum_m\sum_p A_m^{(n)*}(\mathbf{q})A_p^{(n)}(\mathbf{q})\tilde{\phi}^*_{m\mathbf{q}}(\mathbf{g})\tilde{\phi}_{p\mathbf{q}}(\mathbf{g}). \tag{B6}$$

Since $\phi_{00}(\mathbf{r})\equiv 1/\phi^{1/2}\equiv$const [see (2.21)] and since $\phi_{n\mathbf{0}}(\mathbf{r})$, $n\neq 0$ is orthogonal to $\phi_{00}(\mathbf{r})$, we therefore get

$$|\tilde{\psi}_{n\mathbf{0}}(\mathbf{0})|^2=\begin{cases}\phi-O\left(\left(\frac{\rho a}{D_p}\right)^2\right) & \text{for } n=0\\ O\left(\left(\frac{\rho a}{D_p}\right)^2\right) & \text{for } n\neq 0,\end{cases} \tag{B7}$$

$$M(\mathbf{0},t)=e^{-\mu_{00}t}-O\left(\left(\frac{\rho a}{D_p}\right)^2\right), \tag{B8}$$

where

$$\mu_{00}=\rho\frac{S_p}{V_p}\left[1+O\left(\frac{\rho a}{D_p}\right)\right]. \tag{B9}$$

This result is true for *all times*, including times that are very short or very long, as long as $\rho a/D_p$ is small. A similar looking result for $M(\mathbf{0},t)$ already appears in Ref. [15], but its validity was only established there for times t that are either very short or very long.

It is easy to show that (B8) and (B9) are also valid for a nonperiodic porous medium: One merely has to repeat the above considerations starting from the more general expression for $M(\mathbf{k},t)$ in terms of the Fourier transforms $\tilde{\psi}_\mu(\mathbf{k})$ of $\psi_\mu(\mathbf{r})$, namely,

$$M(\mathbf{k},t)=\frac{1}{\phi}\sum_\mu e^{-\mu t}|\tilde{\psi}_\mu(\mathbf{k})|^2, \tag{B10}$$

where

$$\tilde{\psi}_\mu(\mathbf{k})\equiv\frac{1}{\sqrt{V}}\int_{V_p}dV e^{-i\mathbf{k}\cdot\mathbf{r}}\psi_\mu(\mathbf{r}). \tag{B11}$$

APPENDIX C: SHORT TIME ASYMPTOTICS FOR LARGE ρ

In Ref. [14] the short time asymptotic behavior of $D(t)$ was analyzed for the case $\rho t\ll(D_pt)^{1/2}\ll a$, which we will call the small ρ regime [see Eqs. (29) and (39) of Ref. [14]]. Other cases studied there were $(D_pt)^{1/2}\ll a$, $\rho=\infty$, and the special case of an isolated spherical pore in that same limit [see Eqs. (51) and (52) of Ref. [14]]. Here we study the case $(D_pt)^{1/2}\ll\rho t\ll a$ when ρ is large but finite, which we will call the large ρ regime. We were not able to include the effects of finite radii of curvature of the interface.

We consider an infinite, d-dimensional half space filled with a homogeneous fluid and bounded by a flat, $(d-1)$-dimensional hyperplane $x=0$, at which the boundary condition (1.2) applies. The d-dimensional diffusion propagator $G_d(\mathbf{r},\mathbf{r}',t)$ is then a product of one-dimensional propagators, $d-1$ of which are free or infinite medium propagators, such as

$$G_0(y,y',t)=\left(\frac{1}{4\pi D_pt}\right)^{1/2}e^{-\frac{(y-y')^2}{4D_pt}}, \tag{C1}$$

while the remaining one $G_1(x,x',t)$ includes the effects of the boundary. That propagator can be written in closed form using the error function, but it is even simpler to use its Laplace transform $\mathcal{L}(G_1(x,x',t))\equiv\tilde{G}_1(x,x',s)$

$$\tilde{G}_1(x,x',s)=\frac{1}{2(sD_p)^{1/2}}\left[e^{-(s/D_p)^{1/2}|x-x'|}+\frac{(sD_p)^{1/2}-\rho}{(sD_p)^{1/2}+\rho}e^{-(s/D_p)^{1/2}(x+x')}\right]. \tag{C2}$$

The total magnetization $M(t)\equiv M(\mathbf{k}=0,t)$ is calculated as follows:

$$\begin{aligned}M(t)&=\frac{1}{V_p}\int_{x>0}d^dr\int_{x'>0}d^dr'G_d(\mathbf{r},\mathbf{r}',t)\\&=\frac{1}{V_p}\int_{x>0}d^dr\int_0^\infty dx'G_1(x,x',t)\\&=\mathcal{L}^{-1}\left[\frac{1}{V_p}\int_{x>0}d^dr\int_0^\infty dx'\tilde{G}_1(x,x',s)\right],\end{aligned} \tag{C3}$$

where $\mathcal{L}^{-1}$ denotes the inverse Laplace transform and the $d-1$ components of $\mathbf{r}'$ that are perpendicular to the x axis have been integrated over explicitly. The integration over x' is also quite straightforward, leading to

$$\int_0^\infty dx'\,\tilde{G}_1(x,x',s)=\frac{1}{s}-\frac{1}{s}\frac{\rho e^{-(s/D_p)^{1/2}x}}{(sD_p)^{1/2}+\rho}. \tag{C4}$$

In the subsequent d-dimensional integration over $\mathbf{r}$ the first term of (C4) yields a boundary independent result—the same result that would be found in the absence of a boundary—while the second term yields a result that is proportional to the surface-to-volume ratio S_p/V_p of the half space, which is henceforth interpreted as the surface-to-volume ratio of the actual physical pore space. We thus get

$$\mathcal{L}(M(t))=\frac{1}{s}-\frac{S_p}{V_p}\frac{D_p^{1/2}\rho}{s^{3/2}[(sD_p)^{1/2}+\rho]}. \tag{C5}$$

While this Laplace transform can be inverted to give $M(t)$ in terms of error functions, we prefer to first expand around $\rho=\infty$. We note in passing that if we expand (C5) in powers of ρ, we easily get the same expansion that was obtained in Ref. [14] for $M(t)$. Expanding (C5) in powers of $1/\rho$ and inverting, we get

$$\mathcal{L}(M(t))=\frac{1}{s}-\frac{S_p}{V_p}\left[\frac{D_p^{1/2}}{s^{3/2}}-\frac{D_p}{s\rho}+\frac{D_p^{3/2}}{s^{1/2}\rho^2}+\cdots\right], \tag{C6}$$

$$M(t) = 1 - \frac{S_p}{V_p}\left[2\left(\frac{D_p t}{\pi}\right)^{1/2} - \frac{D_p}{\rho} + \frac{D_p}{\rho^2}\left(\frac{D_p}{\pi t}\right)^{1/2} + \cdots\right]. \quad \text{(C7)}$$

From (1.6), we easily get that

$$6D(t)t = -\left[\nabla_{\mathbf{k}}^2\left(\frac{M(\mathbf{k},t)}{M(t)}\right)\right]_{\mathbf{k}=0} = \frac{1}{M(t)}\frac{1}{V_p}\int_{x>0} d^d r \times \int_{x'>0} d^d r'(\mathbf{r}-\mathbf{r}')^2 G_d(\mathbf{r},\mathbf{r}',t). \quad \text{(C8)}$$

In order to evaluate the integral over $\mathbf{r}'$, we again first integrate over the $d-1$ components that are perpendicular to the x axis to get

$$\int_{x'>0} d^d r'(\mathbf{r}-\mathbf{r}')^2 G_d(\mathbf{r},\mathbf{r}',t) = \int_0^\infty dx'\,[(x-x')^2 + 2(d-1)D_p t]G_1(x,x',t). \quad \text{(C9)}$$

The Laplace transform of this result is

$$\int_0^\infty dx'\left[(x-x')^2 - 2(d-1)D_p\frac{\partial}{\partial s}\right]\tilde{G}_1(x,x',s) = \frac{2dD_p}{s^2} - \frac{e^{-\left(\frac{s}{D_p}\right)^{1/2}x}}{2(sD_p)^{1/2}}\left[\frac{2\rho}{(sD_p)^{1/2}+\rho}\times\left(\frac{D_p x^2}{(sD_p)^{1/2}} + \frac{(d+1)D_p x}{s} + \frac{2dD_p^3}{(sD_p)^{3/2}}\right) + \frac{4D_p x}{s}\frac{(sD_p)^{1/2}-\rho}{(sD_p)^{1/2}+\rho} + \frac{2(d-1)D_p^2\rho}{s[(sD_p)^{1/2}+\rho]^2}\right]. \quad \text{(C10)}$$

The $\int d^d r$ integration can now be applied to this result to yield

$$\mathcal{L}(2dM(t)D(t)t) = \frac{2dD_p}{s^2} - \frac{S_p}{V_p}\frac{D_p}{s^2}\left[\frac{3(d+1)D_p\rho}{(sD_p)^{1/2}[(sD_p)^{1/2}+\rho]} + \frac{2D_p}{(sD_p)^{1/2}}\frac{(sD_p)^{1/2}-\rho}{(sD_p)^{1/2}+\rho} + \frac{(d-1)D_p\rho}{[(sD_p)^{1/2}+\rho]^2}\right]. \quad \text{(C11)}$$

As before, this Laplace transform is best expanded for either small or large ρ before inverting. The small ρ expansion leads to the same results as found in Ref. [14]. The large ρ expansion leads to

$$2d[M(t)D(t) - D_p]t = -2dD_p t\frac{S_p}{V_p}\left[\frac{2(3d+1)}{3d}\left(\frac{D_p t}{\pi}\right)^{1/2} - \frac{D_p}{\rho} + \frac{d+1}{d}\frac{D_p}{\rho^2}\left(\frac{D_p}{\pi t}\right)^{1/2} + \cdots\right]. \quad \text{(C12)}$$

Using (C7), we now get the following expression for the time-dependent diffusion coefficient $D(t)$, defined by (1.6):

$$\frac{D(t)}{D_p} \approx 1 - \frac{S_p/V_p}{1+\frac{S_p}{V_p}\frac{D_p}{\rho}}\left[\frac{2}{3d}\left(\frac{D_p t}{\pi}\right)^{1/2} + \frac{1}{d}\frac{D_p}{\rho^2}\left(\frac{D_p}{\pi t}\right)^{1/2}\right] - \left(\frac{S_p/V_p}{1+\frac{S_p}{V_p}\frac{D_p}{\rho}}\right)^2\left[\frac{2}{3d}\frac{D_p t}{\pi} + \frac{2(3d+1)}{3d}\frac{D_p^2}{\pi\rho^2}\right] \quad \text{for} \quad (D_p t)^{1/2} \ll \rho t \ll a. \quad \text{(C13)}$$

The leading deviations from 1 on the right-hand side of both (C7) and (C13), namely, the terms of order $(D_p t)^{1/2} S_p/V_p$ which remain when $\rho = \infty$, are identical to the results of Ref. [14]. It is also important to note again that we have not included any corrections that arise from microgeometrical details other than S_p/V_p, such as the local radii of curvature of the interface.

[1] R.C. Wayne and R.M. Cotts, Phys. Rev. **151**, 264 (1966).
[2] P.T. Callaghan, A. Coy, D. MacGowan, K.J. Packer, and F.O. Zelaya, Nature **351**, 467 (1991).
[3] P.T. Callaghan, D. MacGowan, K.J. Packer, and F.O. Zelaya, Magn. Reson. Imaging **9**, 663 (1991).
[4] P.T. Callaghan, A. Coy, T.P.J. Halpin, D. MacGowan, K.J. Packer, and F.O. Zelaya, J. Chem. Phys. **97**, 651 (1992).
[5] P.T. Callaghan, *Principles of Nuclear Magnetic Resonance Microscopy* (Oxford University Press, Oxford, 1991); this book describes most of the relevant experimental and theoretical research in the field of NMR in porous media which was done before 1990, including references.
[6] W.E. Kenyon, Nucl. Geophys. **6**, 153 (1992).
[7] B. Robertson, Phys. Rev. **151**, 273 (1966).
[8] C.H. Neuman, J. Chem. Phys. **60**, 4508 (1974).
[9] K.R. Brownstein and C.E. Tarr, Phys. Rev. A **19**, 2446 (1979).
[10] M.H. Cohen and K.S. Mendelson, J. Appl. Phys. **53**, 1127 (1982).
[11] J.R. Banavar and L.M. Schwartz, in *Molecular Dynamics in Restricted Geometries*, edited by J. Klafter and J.M. Drake (Wiley, New York, 1989), p. 273.
[12] P.P. Mitra, P.N. Sen, L.M. Schwartz, and P. Le Doussal, Phys. Rev. Lett. **68**, 3555 (1992).
[13] P.P. Mitra and P.N. Sen, Phys. Rev. B **45**, 143 (1992).
[14] P.P. Mitra, P.N. Sen, and L.M. Schwartz, Phys. Rev. B

47, 8565 (1993).
[15] P.N. Sen, L.M. Schwartz, P.P. Mitra, and B.I. Halperin, Phys. Rev. B **49**, 215 (1994).
[16] D.J. Bergman and K.J. Dunn, Phys. Rev. B **50**, 9153 (1994).
[17] K.J. Dunn and D.J. Bergman, J. Chem. Phys. (to be published).
[18] D.J. Bergman and K.J. Dunn, Phys. Rev. B **45**, 13 262 (1992).
[19] M.D. Hürlimann, L.L. Latour, and C.H. Sotak, Magn. Reson. Imaging **12**(2), 325 (1994).
[20] Y.M Strelniker and D.J. Bergman, Phys. Rev. B **50**, 14001 (1994).
[21] D.J. Bergman, K.J. Dunn, L.M. Schwartz, and P.P. Mitra, preceding paper, Phys. Rev. E **51**, 3393 (1995).